Folding Mechanism of the *Tetrahymena* Ribozyme P4−P6 Domain†

Michael L. Deras,‡ Michael Brenowitz,§,|| Corie Y. Ralston,§,⊥ Mark R. Chance,§,⊥ and Sarah A. Woodson*,‡

Thomas C. Jenkins Department of Biophysics, Johns Hopkins University, 3400 North Charles Street, Baltimore, Maryland 21218-2685, and Center for Synchrotron Biosciences, and Department of Biochemistry, and Department of Physiology and Biophysics, Albert Einstein College of Medicine of Yeshiva University, 1300 Morris Park Avenue, Bronx, New York 10461

Received May 3, 2000; Revised Manuscript Received June 23, 2000

ABSTRACT: Synchrotron X-ray-dependent hydroxyl radical footprinting was used to probe the folding kinetics of the P4−P6 domain of the *Tetrahymena* group I ribozyme, which forms a stable, closely packed tertiary structure. The 160-nt domain folds independently at a similar rate ($\sim$2 s^{-1}) as it does in the ribozyme, when folding is measured in 10 mM sodium cacodylate and 10 mM $MgCl_2$. Surprisingly, tertiary interactions around a three-helix junction (P5abc) within the P4−P6 domain fold at least 25 times more rapidly ($k \geq 50$ s^{-1}) in isolation, than when part of the wild-type P4−P6 RNA. This difference implies that long-range interactions in the P4−P6 domain can interfere with folding of P5abc. P4−P6 was observed to fold much faster at higher ionic strength than in 10 mM sodium cacodylate. Analytical centrifugation was used to measure the sedimentation and diffusion coefficients of the unfolded RNA. The hydrodynamic radius of the RNA decreased from 58 to 46 Å over the range of 0−100 mM NaCl. We propose that at low ionic strength, the addition of Mg^{2+} causes the domain to collapse to a compact intermediate where P5abc is trapped in a non-native structure. At high ionic strength, the RNA rapidly collapses to the native structure. Faster folding most likely results from a different average initial conformation of the RNA in higher salt conditions.

Recent work on the folding kinetics of catalytic RNAs has revealed the presence of multiple folding pathways (*1*, *2*). Some pathways lead directly to the native state, while others result in "kinetically trapped" conformations that contain some native, as well as non-native interactions (*3*−*5*). These partially misfolded intermediates, which are represented by local minima on an energy landscape, must overcome significant activation barriers to reach the native state. As a result, the overall folding times for large RNAs are typically in the range of seconds to minutes (reviewed in ref *6*).

In contrast, individual domains of tertiary structure have been observed to fold on time scales of 0.1−1 s. For example, tertiary structure in the catalytic domain of the ribozyme from *Bacillus subtilis* RNase P forms at a rate of $\sim$10 s^{-1} at 37 °C when folding is induced by the addition of Mg^{2+} (*7*). A domain of the *Tetrahymena* ribozyme, containing paired (P) regions P4−P6[1] (Figure 1) folds at a rate of $\sim$1 s^{-1} at 42 °C (*8*). Nucleotides in P3, P7, and P9, which form the catalytic center of the ribozyme, reach the native conformation approximately 100 times more slowly (*8*, *9*).

The rapid folding of individual domains provides an opportunity to study fast folding mechanisms in more detail. The 160-nt P4−P6 domain of the *Tetrahymena* ribozyme folds independently, and the structure of the isolated domain is very similar to its structure in the full-length ribozyme (*10*, *11*). The RNA makes a 150° bend at the nucleotides that join helices P5 and P5a in the presence of Mg^{2+} (J5/5a; Figure 1). This bend permits close packing of the two halves of the domain. A high-resolution X-ray structure (*12*) revealed specific tertiary contacts between an A-rich bulge and the coaxially stacked P4−P5−P6 helices and between a GAAA tetraloop in P5 and a tetraloop receptor motif in P6a (*10*, *11*). Local tertiary interactions around the junction between helices P5a, P5b, and P5c define a subdomain of tertiary structure (P5abc) that also folds independently of the rest of the ribozyme (*11*, *13*).

Time-resolved hydroxyl radical footprinting using a synchrotron X-ray source has been used to simultaneously monitor the rate of formation of individual tertiary contacts with millisecond time resolution (*8*). In this method, solvent-exposed regions of the RNA backbone are susceptible to ribose oxidation and strand cleavage in the presence of hydroxyl radical, while residues that are on the interior of a folded RNA are protected from cleavage (*14*−*16*). Irradiation of aqueous solutions with a high-intensity synchrotron white

† This work was supported by grants from the NIH RO1-GM60819, RO1-GM39929, S10-RR13851, and P41-RR01633. Research was carried out, in part, at the National Synchrotron Light Source, Brookhaven National Laboratory, which is supported by the U.S. Department of Energy, Division of Materials Sciences and Division of Chemical Sciences.

* To whom correspondence should be addressed. Phone (410) 516-2015; fax (410) 516-4118; e-mail: swoodson@jhu.edu.

‡ Department of Biophysics, Johns Hopkins University.

§ Center for Synchrotron Biosciences, Albert Einstein College of Medicine.

|| Department of Biochemistry, Albert Einstein College of Medicine.

⊥ Department of Physiology and Biophysics, Albert Einstein College of Medicine.

[1] Abbreviations: P4−P6, paired helices 4, 5, and 6 of the *Tetrahymena* ribozyme; EDTA, ethylenediamine tetraacetic acid.

10.1021/bi0010118 CCC: $19.00
Published on Web 08/15/2000

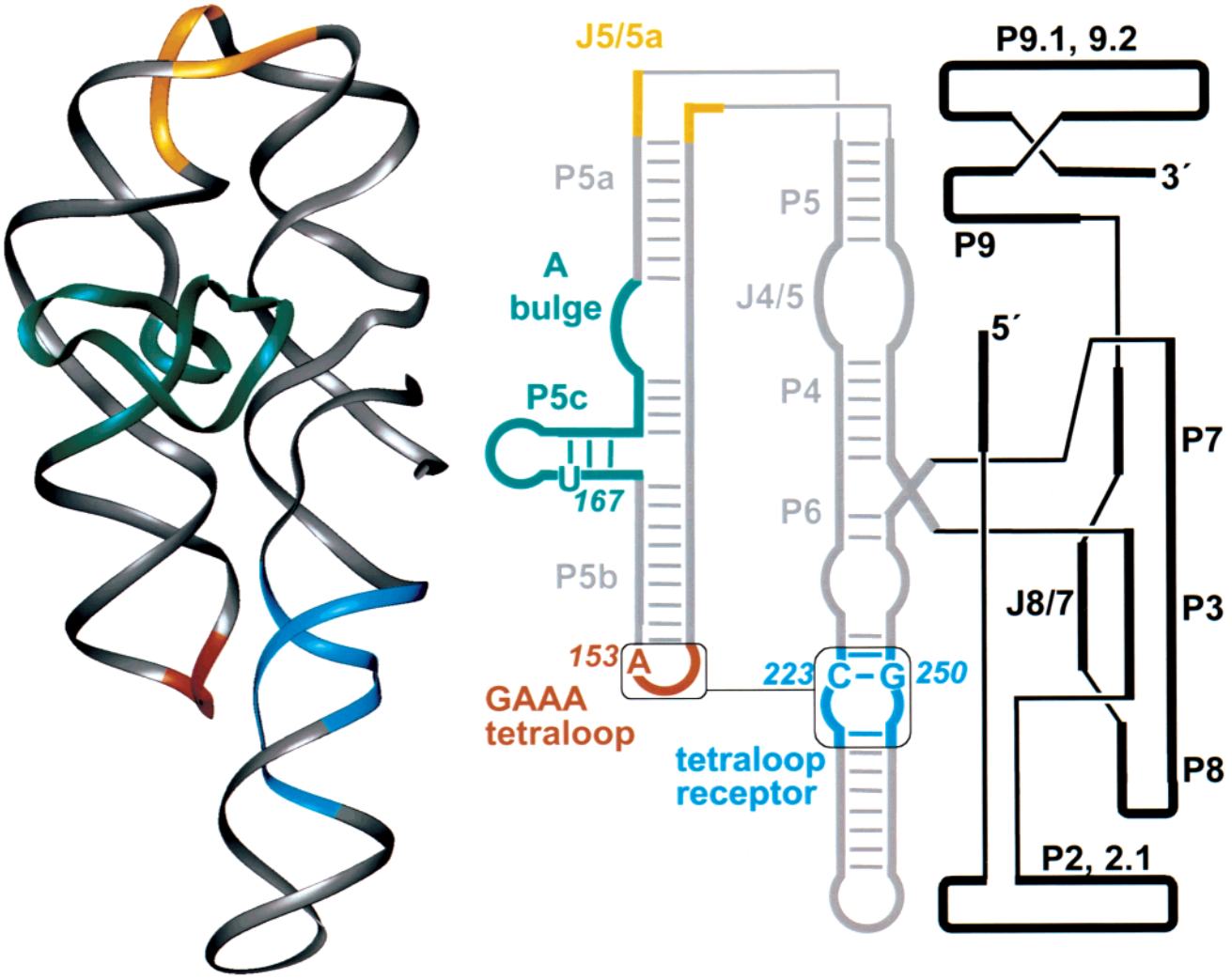

FIGURE 1: (a) Ribbon diagram of the P4−P6 domain (160 nt) (*12*). (b) Secondary structure of the *Tetrahymena* ribozyme (*45*). In gray are the pairings of the P4−P6 domain, the remainder of the *Tetrahymena* ribozyme is shown schematically in black. Paired (P) regions are numbered 5′ to 3′. The three-helix junction of P5abc is shown in green, the GAAA tetraloop is shown in red, the 11-nt conserved tetraloop receptor is shown in blue, and the unpaired sequences of J5/5a are shown in yellow.

X-ray beam produces sufficient concentrations of hydroxyl radical to carry out cleavage reactions in as little as 10 ms (*17*).

Nucleotides that are excluded from solvent by tertiary interactions in the P4−P6 domain (*12*) were protected from hydroxyl radical cleavage at a rate of ~1 s^{-1} in buffer containing 10 mM sodium cacodylate at 42 °C (*8*). The rate constants determined for each protected region were very similar, indicating that interactions between the two halves of the P4−P6 domain form in a concerted manner. Residues within the P5abc subdomain were protected slightly faster, ~2 s^{-1} (*8*), raising the possibility that folding occurred in two transitions, with the three-helix junction in P5abc folding as the first step.

In this study, we have probed the folding mechanism of the P4−P6 domain alone, using time-resolved hydroxyl radical footprinting. In a complementary study, global changes in the conformation of P4−P6 RNA were monitored with 1 ms dead time using changes in the fluorescence emission of pyrene covalently attached to U107, near the 5′ end of the RNA (*18*, *19*). We show that tertiary interactions in the P4−P6 RNA form in a concerted manner, rather than in sequence. We also demonstrate that an RNA containing only the P5abc three helix junction folds 25 times more rapidly than the wild-type P4−P6 domain, implying that interactions with P4 and P6 inhibit folding of P5abc under these conditions. These results suggest that non-native yet compact conformations compete with the native structure, resulting in longer folding times. Increasing concentrations of Na^+ accelerate the rate of folding by apparently allowing the RNA to bypass non-native intermediates during folding. This model is supported by the results of analytical centrifugation experiments that probe the global conformation of the unfolded RNA.

MATERIALS AND METHODS

RNA Preparation. Plasmids encoding a 160-nt P4−P6 RNA (wt; J5/5a paired; A153G; C223A:G250U) were generously provided by F. Murphy and T. Cech (*10*, *11*). P4−P6:U167C RNA was prepared by S. Silverman. Plasmid encoding P5abc was a gift of E. Doherty and J. Doudna (*13*). RNAs were prepared by in vitro transcription using T7 RNA polymerase as previously described (*20*). Transcripts were purified by excision from preparative denaturing 4% polyacrylamide gels. The RNA was treated with calf alkaline intestinal phosphatase (New England Biolabs) prior to

Table 1: Mg^{2+}-dependence of P4−P6 Domain Tertiary Structure[a]

	wild type		J5/5a paired[b]		A153G[b]		C223A;G250U[b]	
nucleotide	$[Mg^{2+}]_{1/2}$	n_H	$[Mg^{2+}]_{1/2}$	n_H	$[Mg^{2+}]_{1/2}$	n_H	$[Mg^{2+}]_{1/2}$	n_H
139−140	0.36 ± 0.01	3.0 ± 0.2						
153−155	0.48 ± 0.01	4.8 ± 0.5						
162−164	0.38 ± 0.01	3.7 ± 0.3	0.25 ± 0.01	2.7 ± 0.4	0.22 ± 0.03	2.8 ± 0.7	0.36 ± 0.04	2.0 ± 0.4
175−177	0.28 ± 0.03	3.0 ± 0.7	0.24 ± 0.02	3.7 ± 1.2	0.22 ± 0.02	3.1 ± 1	0.26 ± 0.04	3.8 ± 2.2
180−181	0.3 ± 0.01	3.5 ± 0.2	0.27 ± 0.02	2.4 ± 0.4	0.21 ± 0.02	3.9 ± 1.3	0.33 ± 0.05	2.7 ± 0.9
185−187	0.38 ± 0.02	3.7 ± 0.5						
200−201	0.57 ± 0.03	5.8 ± 1.6						
212−215	0.65 ± 0.05	4.2 ± 1.3						

[a] Midpoints and Hill constants were obtained from fits of fractional saturation versus $MgCl_2$ concentration (mM) to the Hill equation as in Figure 2, in 10 mM sodium cacodylate, pH 7.5, 10 mM $MgCl_2$, and 1 mM EDTA at 42 °C. Data were obtained as described in Materials and Methods. [b] Only three positions are protected from hydroxyl radical cleavage in the J5/5a paired RNA. The protection pattern of A153G and C223A;G250U mutant RNAs more closely resembles that of the wild type above 30 mM $MgCl_2$ (*10*).

labeling with γ-[^{32}P]-ATP (NEN) and polynucleotide kinase (New England Biolabs). The ^{32}P-labeled RNA was repurified by preparative gel electrophoresis and dissolved in 10 mM Tris·HCl, pH 7.5, and 1 mM EDTA (TE) before use.

Fe(II)-EDTA-Dependent Hydroxyl Radical Footprinting. Reactions were performed as described previously (*16*). 5′-^{32}P-labeled RNA was diluted in 10 μL 10 mM sodium cacodylate, pH 7.5, and 0.1 mM EDTA (CE) (20 000 cpm/μL). The RNA was annealed by placing 4 μL of 50 mM $MgCl_2$ or water underneath the lid of the microfuge tube, heating to 95 °C for 1 min, and centrifuging immediately. Samples were equilibrated for 5 min on ice before adding 2 μL of 2.5 mM $(NH_4)_2Fe(SO_4)_2$ and 5 mM EDTA (pH 8.0), 2 μL of 10 mM sodium L-ascorbate, and 2 μL of 0.3% H_2O_2 (20 μL total). Reactions were quenched after 2 min with 2 μL of 100 mM thiourea. The RNA was precipitated at −80 °C for 15 min with 300 mM sodium acetate (pH 5.0), 0.66 μg of carrier tRNA, 4 mM EDTA, and 3 vol of ethanol. Samples were pelleted, dried, and dissolved in 6 μL of 1× TBE loading buffer with 5 M urea. Before loading on denaturing 8% polyacrylamide gels, each sample was heated to 95 °C for 1 min, then immediately chilled on ice. Dried gels were exposed to Molecular Dynamics Phosphorimager screens and quantified using ImageQuant for Macintosh version 1.11.

Synchrotron X-ray-Dependent Hydroxyl Radical Footprinting. The time-dependence of hydroxyl radical protection was measured as previously reported at beamline X9a of the National Synchrotron Light Source (*17, 21*). Experiments were conducted at a constant temperature of 42 °C, and a final concentration of 10 mM $MgCl_2$. Following irradiation for 10−50 ms (depending on the natural decay of the X-ray ring current), the RNA was recovered by ethanol precipitation as described for Fe(II)EDTA reactions. The activity of protected regions in the sequencing gel was normalized to the activity of unprotected regions to correct for variations in sample recovery and loading. This ratio of protection was plotted versus time and fit to a single-exponential $\bar{Y} = 1 - \exp(-kt)$ to determine k_{obs}. Rates are given as the mean of at least three experiments, along with the standard error.

Equilibrium Mg^{2+} Titrations. A total of 55 μL of RNA (~1 μCi) was annealed at 95 °C for 1 min and then distributed in 5-μL portions to microfuge tubes with increasing concentrations of $MgCl_2$ in CE buffer to a final volume of 25 μL. Each tube was then equilibrated at 42 °C in a temperature-controlled block facing the X-ray beam and exposed using a computer-controlled shutter for 50−80 ms (*21*). The samples were then recovered and analyzed as described above. The relative protection was plotted versus Mg^{2+} concentration and fit to the Hill model (*22*).

Analytical Ultracentrifugation. Sedimentation velocity studies were conducted in a Beckman XL-I analytical ultracentrifuge at 40 000 rpm. Unlabeled gel-purified RNA was diluted to 300 μL in CE plus the indicated concentration of NaCl and annealed for 3 min at 95 °C as described above. The contribution of 9.4 mM Na^+ from the CE buffer is calculated using the Henderson−Hasselbalch equation at pH 7.5 and a pK_a = 6.27 for cacodylic acid. The samples and rotor were equilibrated at 12 °C before each run. The sedimentation boundary was monitored by optical absorption at 260 nm. RNA concentrations were calculated using $\epsilon_{\mu g/mL} = 0.027$. The sedimentation boundaries were analyzed as *dc*/*R* using SVEDBERG v6.37 (*23*) to determine the sedimentation coefficient, *S*, and the diffusion coefficient, *D*. No fewer than 12 and as many as 60 absorbance scans were globally analyzed for each experiment. The observed values were normalized to standard conditions of 20 °C and water ($S_{20,w}$ and $D_{20,w}$) by correcting for solvent density and viscosity. A value for the partial specific volume, $\bar{v}$, of 0.53 $cm^3\ g^{-1}$ (*24*) was used in the calculation of apparent molecular weights.

RESULTS

X-ray Footprinting of P4−P6 RNA. Tertiary structure in a 160-nt RNA containing helices P4−P6 of the *Tetrahymena* ribozyme was monitored by changes in hydroxyl radical cleavage of the RNA as previously described (*8*). The protection pattern of the fully folded P4−P6 RNA observed by X-ray footprinting is identical to that obtained in experiments in which hydroxyl radical was generated with Fe(II)-EDTA (*10*) and is a subset of the protection pattern of the full-length ribozyme (*16*). Thus, the P4−P6 domain is correctly folded under the conditions of these experiments.

The thermodynamic stability of P4−P6 was determined from Mg^{2+}-dependent folding isotherms in CE at 42 °C (*25*). The K_d and Hill constants (n_H) determined for each protected site in the wild-type P4−P6 RNA were within error of each other, K_d = 0.3 mM and $n_H \approx 4$ (Table 1). Thus, the equilibrium folding transition of P4−P6 is concerted with respect to Mg^{2+} concentration. These isotherms are more cooperative than those observed in folding of the full-length ribozyme, where K_d = 0.2 mM and n_H = 2.4 (*25*). The 10

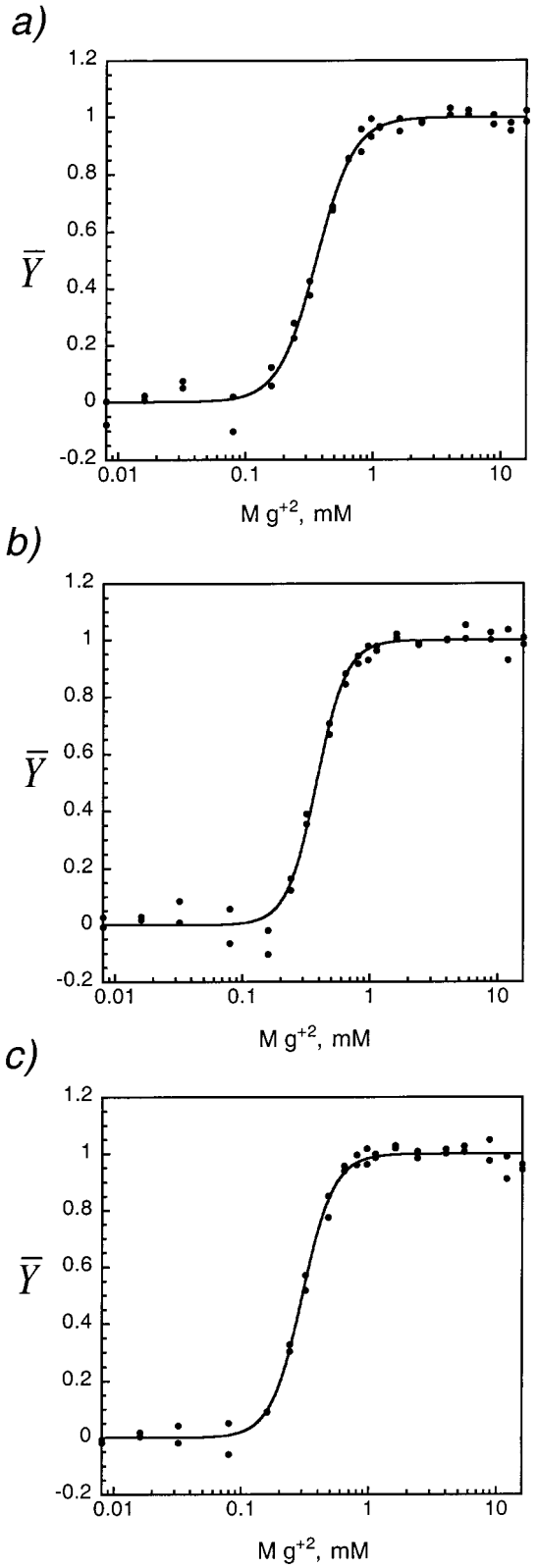

FIGURE 2: Magnesium-dependence of tertiary folding by X-ray hydroxyl radical footprinting. Wild-type P4−P6 RNA was equilibrated at 42 °C in 10 mM sodium cacodylate, pH 7.5, 1 mM EDTA (CE) plus various $MgCl_2$ concentrations, before exposure to the X-ray beam. The relative extent of protection at each site, $\bar{Y}$, was fit to the Hill model. The parameters of the fits are given in Table 1. (a) nt 139−140; (b) nt 163−164.; (c) nt 180−181.

mM $MgCl_2$ used in the folding kinetics experiments described below is sufficiently high (Figure 2) so that unfolding contributes negligibly to the observed rate constants.

Table 2: Observed Rates of Protection from Hydroxyl Radical Cleavage (s^{-1})[a]

nt	seq	structure	P4−P6[b]	ribozyme[c]	A153G[b]	C223A; G250C[b]
126−127	GC	P5a	1.8 ± 0.3	0.9 ± 0.5		
139−140	AA	J5a/5b	1.9 ± 0.4	0.9 ± 0.4		
153−155	ACU	P5b	2.5 ± 0.5	1.3 ± 0.5		
162−164	UGC	P5c	1.9 ± 0.3	1.6 ± 0.8	1.9 ± 0.5	2.4 ± 0.7
169	G	L5c	2.1 ± 0.3	2.0 ± 0.7		
175−177	GGU	P5c	1.7 ± 0.4	2.7 ± 1.5	3.1 ± 0.8	2.9 ± 0.3
180−181	GG		1.5 ± 0.3	1.8 ± 0.6	2.9 ± 0.6	2.6 ± 0.3
185−187	UAA	A-bulge	1.7 ± 0.4	0.9 ± 0.3		
195−196	GA	P5a	2.1 ± 0.6	nd[d]		
200−201	GG	P5	1.8 ± 0.2	1.0 ± 0.5		
212−215	GCAG	P4/P6	2.5 ± 0.4	0.9 ± 0.5		

[a] Observed rates in 10 mM sodium cacodylate, pH 7.5, 10 mM $MgCl_2$, and 1 mM EDTA at 42 °C were determined as described in Figure 3. [b] 160-nt RNAs containing only the P4−P6 domain. [c] Data on L-21 ribozyme taken from ref *8*. [d] nd, not determined.

Folding rates were obtained from the extent of protection at various times after the formation of tertiary structure was initiated by mixing the RNA with 10 mM $MgCl_2$. Most of the secondary structure of the RNA is stable under our initial conditions of 10 mM sodium cacodylate (CE) at 42 °C (*26*). The relative extent of cleavage at each protected region was fit to a first-order rate equation (Figure 3) and yielded rate constants on the order of 2 s^{-1} at 42 °C (Table 2; Figure 4a). These rates are about twice those of the same sequences in the intact ribozyme under identical experimental conditions (*8*), consistent with essentially independent folding of the P4−P6 domain in the intact ribozyme (*10*, *27*).

The observed rates of protection at each position within the 160-nt P4−P6 RNA were similar to each other, ranging from 1.5 ± 0.3 to 2.5 ± 0.5 s^{-1} (Figure 4a). Despite the improved electrophoretic resolution of data on the smaller P4−P6 RNA (and hence improved precision of the analysis), there is no evidence in these data that P5abc folds more rapidly, as observed with the ribozyme. We conclude that the entire tertiary structure of the P4−P6 domain is formed in a concerted manner at a rate of about 2 s^{-1} under these experimental conditions. This conclusion is in contrast to our earlier suggestion that the three-helix junction folds before other tertiary contacts are established and thus helps nucleate formation of the structure (*8*). The present results suggest that the remaining sequences of the ribozyme have a small inhibitory effect on the rate of P4−P6 folding.

Folding of the P5abc Subdomain. To measure the intrinsic folding rate of the P5abc three-helix junction, X-ray footprinting experiments were carried out on a P4−P6 mutant in which contact between the two halves of the domain is inhibited. Replacement of nucleotides in the region joining P5 and P5a (J5/5a) with a complementary sequence (J5/5a paired) yields a mutant RNA that is incapable of making a 150° bend (Figure 4b) (*10*). Since J5/5a paired RNA cannot form the long-range contacts of the wild type RNA, only residues in P5c are protected from hydroxyl radical cleavage (*10*). However, the protection pattern of P5c is the same as it is in the wild-type P4−P6 RNA, suggesting that the native local tertiary structure of the three-helix junction has been preserved in the mutant. The Mg^{2+}-dependence of P5abc folding was similar in the J5/5a paired and wild-type RNAs (K_d = 0.2−0.3 mM). These values are roughly comparable to those obtained in earlier studies of P5abc (*13*).

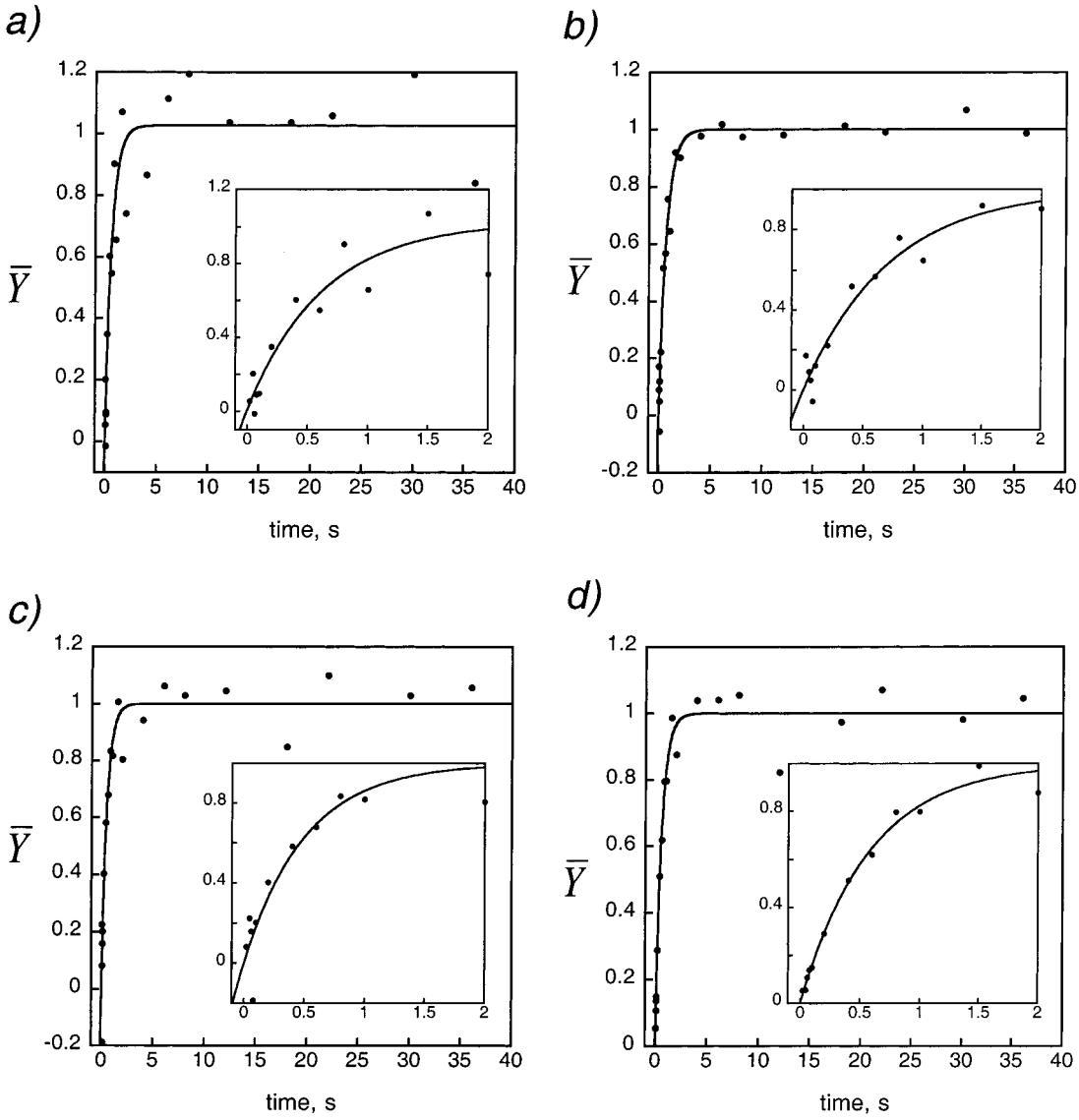

FIGURE 3: Time-resolved X-ray footprinting of the P4−P6 RNA. Relative protection from hydroxyl radical cleavage at each site, $\bar{Y}$, was fit to a first-order rate equation as described in Materials and Methods. Experiments were in CE plus 10 mM $MgCl_2$ at 42 °C. Rate constants are listed in Table 2. (a) P5c (nt 163−164); (b) L5c (nt 169); (c) A bulge (nt 185−187); (d) P5a (nt 200−201). Insets are expansions of the first 2 s of the folding reaction.

Surprisingly, residues that are protected from cleavage by folding of the P5abc subdomain reached the maximum level of protection within the shortest dead time of our assay, which was 30 ms (Figure 5a). This result was confirmed in experiments carried out on a 72-nt RNA comprising only the sequences of the P5abc subdomain (Figures 4B and 5B) (*13*). Folding of the 72-nt P5abc was also complete within the dead time of the experiment. Thus, the three-helix junction folds at least 25 times faster in isolation ($k_{obs} \geq 50$ s^{-1}) than it does when part of the wild-type P4−P6 domain ($k_{obs} = 2$ s^{-1}). This result suggested that folding of P5abc is inhibited by interactions with the P4, P5, and P6 helices in the wild-type RNA, under these experimental conditions.

Conformation of P5abc in Wild-type and Mutant RNAs. We considered several ways to account for differences in the observed folding rates of the P5abc subdomain. The first possibility is that the folded conformation of the three-helix junction is different in the wild-type P4−P6 as compared to J5/5a paired and P5abc. However, the hydroxyl radical protection pattern of these residues is identical for all RNA under these conditions, implying that significant structural differences are unlikely (Figure 6). Moreover, previous chemical modification data showed that a truncated, 56-nt RNA (tP5abc) adopts a tertiary structure that is very similar to the conformations of these sequences in the folded P4−P6 domain (*10*, *13*). Several investigations have shown that prefolded P5abc RNAs may be added in trans to partially deleted ribozymes that lack the subdomain, and this yields catalytically functional RNA (*13*, *28*−*30*). Thus, differences in the folded conformation of P5abc are unlikely to account for the observed folding kinetics.

Secondary Structure Rearrangements. The second possibility is that the wild-type P4−P6 RNA adopts incorrect secondary structures under the initial conditions of our experiments (no Mg^{2+} and 10 mM sodium cacodylate), despite the fact that the RNA was annealed at high temperatures before the start of the folding reaction. In this scenario, the observed folding rate is limited by secondary structure rearrangements rather than by the formation of tertiary interactions. Native gel electrophoresis of P4−P6 RNA did

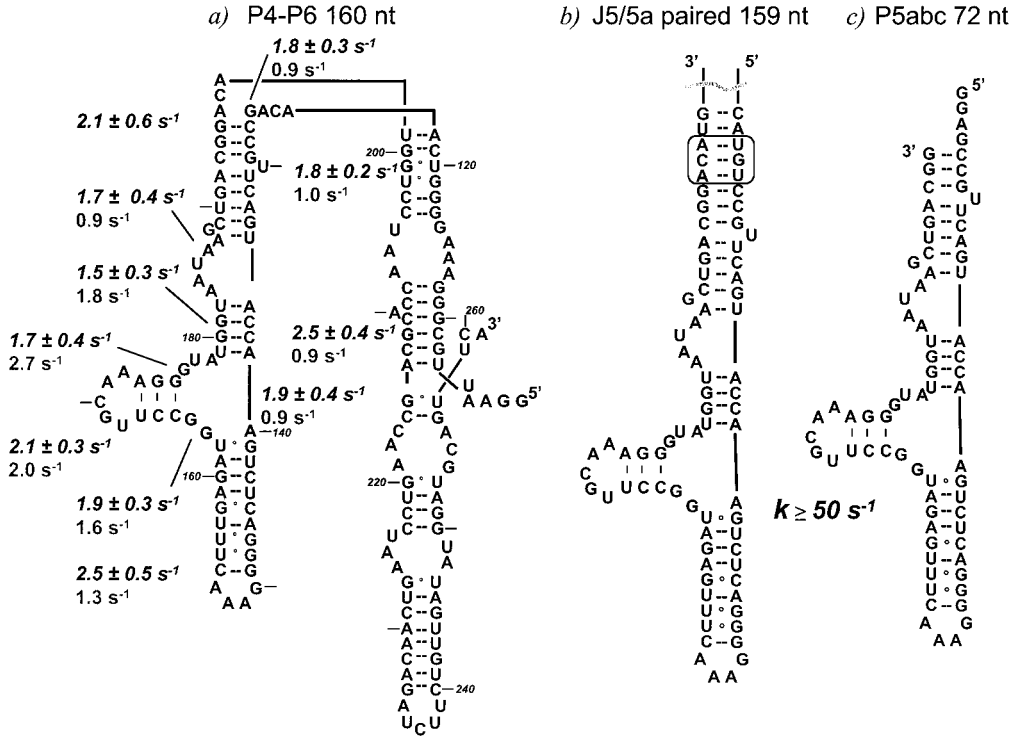

FIGURE 4: Folding kinetics of the P4−P6 domain. Shaded nucleotides are protected from hydroxyl radical cleavage in the presence of 10 mM $MgCl_2$. (a) Comparison of rate constants for folding of P4−P6 domain alone (black; this paper) with folding of the L-21 ribozyme (gray; ref *8*). (b) Protected nucleotides in the P5abc subdomain (shaded in gray) of J5/5a paired RNA. Mutations in region joining P5 and P5a are outlined. Other sequences are not protected from cleavage. Maximum protection was reached within the dead time of the experiment (30 ms). (c) Protected nucleotides in the 72-nt P5abc RNA.

not reveal slowly exchanging conformations in the presence or absence of Mg^{2+}, and nuclease mapping experiments did not provide evidence for alternative secondary structures (data not shown). Earlier efforts to map the secondary structure of the P4−P6 domain also failed to uncover alternative base pairing arrangements for the P4, P5, and P6 helices, under buffer conditions similar to ours (*10*). We conclude that large-scale rearrangements in secondary structure are not the most plausible explanation for slower folding of P5abc in the wild-type P4−P6 RNA.

The preferred structure of the P5c stem-loop in the absence of Mg^{2+} differs, however, from its Mg^{2+}-dependent conformation (*31*). In the absence of Mg^{2+}, a 5-base pair stem and GCAA tetraloop replaces the secondary structure shown in Figure 4. Evidence for this local switch in the secondary structure of P5c was obtained from ^{1}H NMR experiments on tP5abc (*31*) and from dimethyl sulfate modification of the 160-nt P4−P6 RNA (*32*). Since the tertiary structure of the 72-nt P5abc RNA used in this investigation forms within 30 ms in our experiments, the base pairs of P5 must realign within this time scale. Therefore, rearrangement of the P5c secondary structure is not sufficient to account for the slower folding of the P4−P6 RNA.

Tertiary Interactions. The third possibility is that interactions between the two halves of the P4−P6 domain interfere with correct folding of P5abc. This model assumes that bending or flexing of the wild-type P4−P6 RNA, which retains the hinge between P5 and P5a, results in contacts between P5 and P5a that inhibit reorganization of the three-helix junction. These hypothetical compact conformations could inhibit overall folding if they are present in the initial population or if they form at least as fast as the P5abc tertiary structure after mixing with Mg^{2+}.

A prerequisite of this hypothesis is that long-range interactions can form while P5abc is misfolded. To test this possibility, the conformation of RNA containing a mutation in P5c was probed by hydroxyl radical cleavage. The mutation U167 to C stabilizes the secondary structure first observed by ^{1}H NMR of tP5abc in the absence of Mg^{2+} (*31*) and lowers the stability of the folded RNA by at least 1.5 kcal mol^{-1} (*32*). Hydroxyl radical footprinting experiments showed that critical tertiary contacts within P5c are disrupted, since nucleotides 175−177 that are normally protected (*10*) by folding of this stem−loop (*12*) were cleaved in the U167C RNA (data not shown). However, weaker protection of nucleotides in P5a, P5b and P5 was still observed. Analysis by native gel electrophoresis in Mg^{2+} has also shown that U167C RNA migrates nearly, but not equally, as rapidly as the wild type (*32*). Since long-range contacts between P4, P5, and P6 are still formed in U167C RNA despite misfolding of the three-helix junction, it is possible that similar conformations could at least transiently form during folding of the wild-type RNA.

Another plausible intermediate conformation may arise if the interaction between the GAAA tetraloop and the tetraloop "receptor" between P6a and P6b forms prior to folding of P5abc. To evaluate if this long-range contact retards P5abc folding, it was disrupted by a mutation in the tetraloop (A153 to G) or by substitution of a G·C base pair in the receptor (C223A;G250U) (*10*). In 10 mM Mg^{2+}, only nucleotides in P5b and P5c are protected from cleavage in the mutant RNAs (Table 1). The Mg^{2+} dependence of these protections is

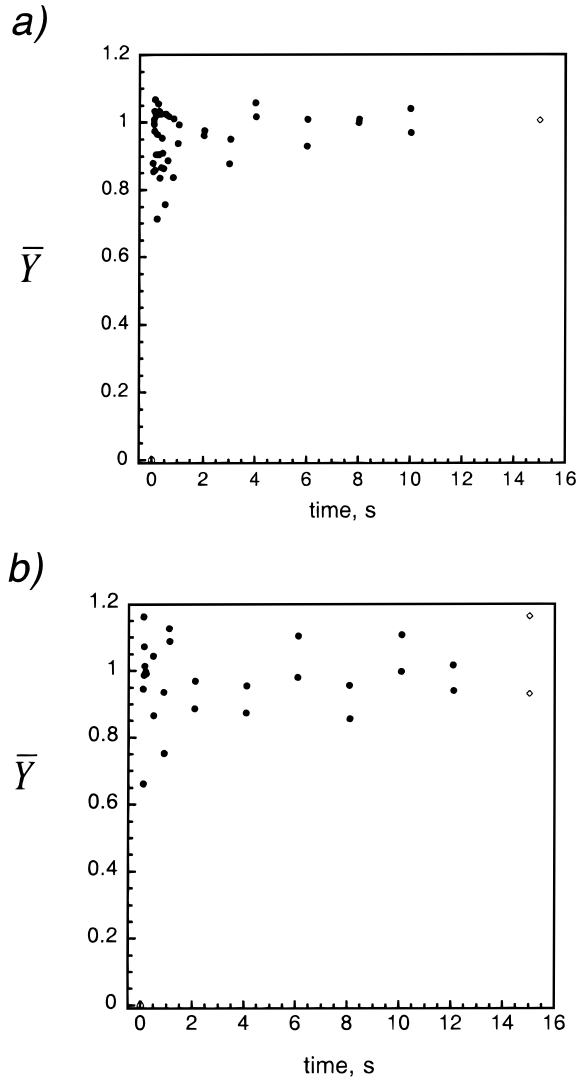

FIGURE 5: Time-resolved footprinting of the P5abc subdomain. Relative protection of nt 180−181 vs time (●) was fit to a first-order rate equation as in Figure 3. (○) Baseline taken before addition of $MgCl_2$; (◊) fully folded RNA that was annealed at 95 °C in 10 mM $MgCl_2$. (a) J5/5a paired RNA. (b) P5abc RNA (72 nt).

identical within experimental error to those of the wild-type RNA. When the folding kinetics were determined, these mutations increased the rates of hydroxyl radical protection to ~3 s^{-1}, about 50% greater than the wild type (Table 2).

Although the tetraloop−receptor interaction stabilizes the native tertiary conformation of the P4−P6 domain, these results show that its presence or absence has only a small effect on the early steps in the folding reaction. Nonetheless, the increase in the folding rates of the mutant RNAs does suggest that P5abc folding is kinetically coupled to the formation of other tertiary interactions within P4−P6. However, the magnitude of the observed change is insufficient by itself to account for the large differences in the folding rates of P4−P6 and J5/5a paired.

Conformation of the Unfolded RNA. Sedimentation velocity experiments were carried out by analytical ultracentrifugation to examine the global hydrodynamic properties of the unfolded wild-type P4−P6 and J5/5a paired RNA. A single component adequately models all the sedimentation boundaries analyzed in these studies. The sedimentation coefficient, *S*, did not decrease with increasing RNA concentration due

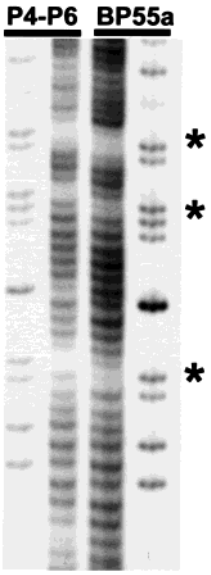

FIGURE 6: Hydroxyl radical cleavage pattern of wild-type P4−P6 domain and J5/5a paired domain. Regions that are protected by tertiary interactions in P5abc are marked with an asterisk. Reactions were carried out using synchrotron X-ray hydroxyl radical footprinting as described in Materials and Methods. G ladder in lanes 1 and 4 from RNase T1. The sequence of J5/5a paired RNA is one nucleotide shorter than the wild type (*10*, *11*). RNA were annealed with 10 mM Mg^{2+} in the manner described for Fe(II)EDTA reactions in Materials and Methods.

to nonideality, as expected. Instead, the observed increase in $S_{20,w}$ with increasing RNA concentration, and corresponding decrease in $D_{20,w}$, is indicative of self-association (Figure 7a). However, at the lowest RNA concentrations examined (which are orders of magnitude greater than those used in the footprinting experiments), the RNA is essentially monomeric. This can be seen in the experimentally determined values of $S_{20,w}$ and $D_{20,w}$ extrapolated to infinite dilution ($S^{\circ}_{20,w}$ and $D^{\circ}_{20,w}$, respectively, Table 3). The diffusion constants calculated from $S^{\circ}_{20,w}$ and the known molecular weights are within error of the experimentally determined values.

In CE buffer, the $S^{\circ}_{20,w}$ and $D^{\circ}_{20,w}$ values obtained for P4−P6 and J5/5a paired are identical within experimental error. The Stokes radius (R_H) and the ratio of the actual frictional coefficient to that expected for a spherical molecule (f/f_o) show that both RNAs are mostly in extended conformations (R_H (wt) = 58 Å; Table 3). If the results are modeled as a prolate ellipsoid, the ratio of the *a* and *b* axes suggest very elongated molecules. These results are unsurprising at the low ionic strength of the CE buffer and argue against stable long-range interactions in unfolded P4−P6 RNA under these conditions.

Ionic Strength. The folding rate of wild-type P4−P6 domain increases dramatically when even low concentrations of NaCl are present in the folding buffer (*19*). This increase in the folding rate is mirrored by a salt-dependent change in the hydrodynamic properties of both P4−P6 and J5/5a paired (Figure 7A; Table 3). Increasing NaCl induces an increase in $S^{\circ}_{20,w}$ and $D^{\circ}_{20,w}$. These changes are reflected in a reduction of R_H and f/f_o, which are indicative of more compact and less elongated average conformations for both P4−P6 and J5/5a paired in 100 mM NaCl (Table 3). Salt-dependent differences in $\bar{v}$ cannot account for the observed sedimentation behavior, since $D^{\circ}_{20,w}$ is not dependent upon $\bar{v}$.

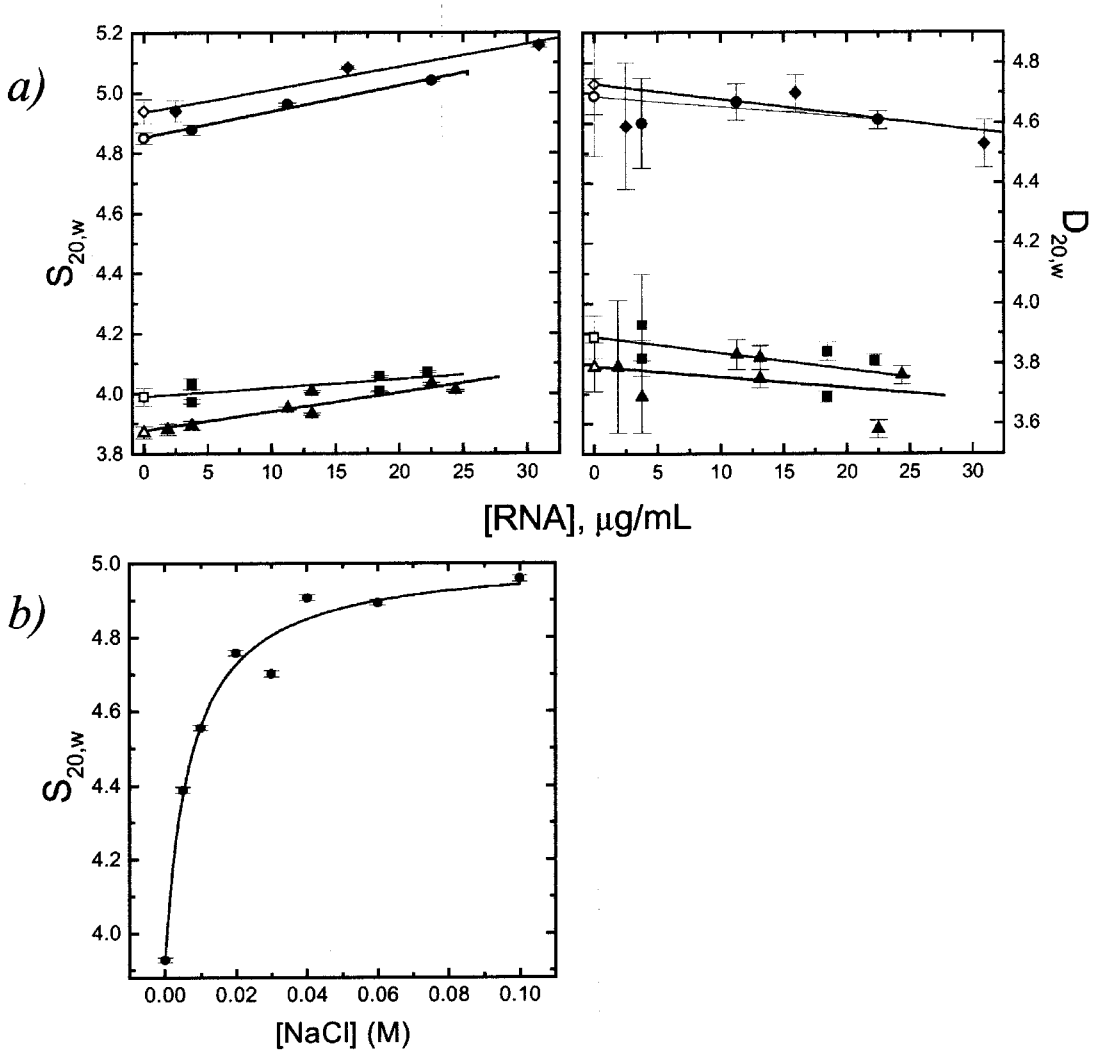

FIGURE 7: Analytical ultracentrifugation. (a) Sedimentation parameters determined for P4−P6 and J5/5a paired as a function of the initial RNA concentration. Experiments were conducted in CE (▲,wild type; ■, J5/5a paired) and CE + 100 mM NaCl buffer (●, wild type; ◆, J5/5a paired). The error bars depict the 95% confidence limits determined from the global analysis of the sedimentation scans selected for analysis for each run. The linear extrapolation of these data to infinite dilution ($S^{\circ}_{20,w}$) is shown by the open symbols; errors were propagated from the experimental measurements (b) $S_{20,w}$ as a function of [NaCl], for wild-type P4−P6 RNA. The solid line depicts the best-fit Langmuir isotherm, with an apparent K_d of 7.3 ± 1.6 mM. The error bars depict the 95% confidence limits of each determination.

Table 3: Sedimentation and Hydrodynamic Parameters for P4−P6 RNA[a]

	0 mM NaCl		100 mM NaCl	
	wt	J5/5a paired	wt	J5/5a paired
	Experimental Values			
$S^{\circ}_{20,w}$ (Svedbergs)	3.88 ± 0.02	3.99 ± 0.03	4.85 ± 0.02	4.94 ± 0.04
$D^{\circ}_{20,w}$ (× 10^7 cm^2/sec)	3.79 ± 0.08	3.89 ± 0.07	4.69 ± 0.06	4.73 ± 0.24
	Calculated Values[b]			
$D^{\circ}_{20,w}$ (× 10^7 cm^2/sec)	3.67 ± 0.04	3.82 ± 0.03	4.63 ± 0.03	4.76 ± 0.03
f/f_o	2.55 ± 0.01	2.47 ± 0.02	2.05 ± 0.01	2.01 ± 0.02
R_H (Å)	57.6 ± 0.3	55.6 ± 0.4	46.3 ± 0.02	45.2 ± 0.03
a/b ratio of anhydrous prolate ellipsoid	38.5 ± 0.4	36.1 ± 0.5	24.1 ± 0.3	22.9 ± 0.4

[a] $S^{\circ}_{20,w}$ and $D^{\circ}_{20,w}$ were measured by analytical centrifugation. $D^{\circ}_{20,w}$ was also calculated from $S^{\circ}_{20,w}$ and the monomer molecular weights of the RNA molecules from the Svedberg equation. Inspection of the Svedberg equation shows that the determination of any two of the parameters S, D, and M_w allows the calculation of the third. The experimentally determined values were used to calculate the Stokes radius, R_H, the ratio of the frictional coefficient and the coefficient expected for a spherical molecule of the known molecular weight, f/f_0, and the ratio, a/b, of the prolate ellipsoid corresponding to a molecule of characterized by R_H and f/f_o. The errors in $S^{\circ}_{20,w}$ and $D^{\circ}_{20,w}$ were propagated from the experimental measurements shown in Figure 7a. [b] Molecular weights of P4−P6 RNAs were calculated from their nucleotide composition, as M_w = 54 492 (wild type) and M_w = 54 125 (J5/5a paired).

The sedimentation behavior of P4−P6 as a function of NaCl concentration was investigated by conducting a NaCl titration at a fixed concentration of RNA (Figure 7b). The transition from the "low-salt" to "high-salt" conformation of P4−P6 has an apparent K_d of 7.3 ± 1.6 mM. This corresponds closely to the Na^+-dependence of the accelerated

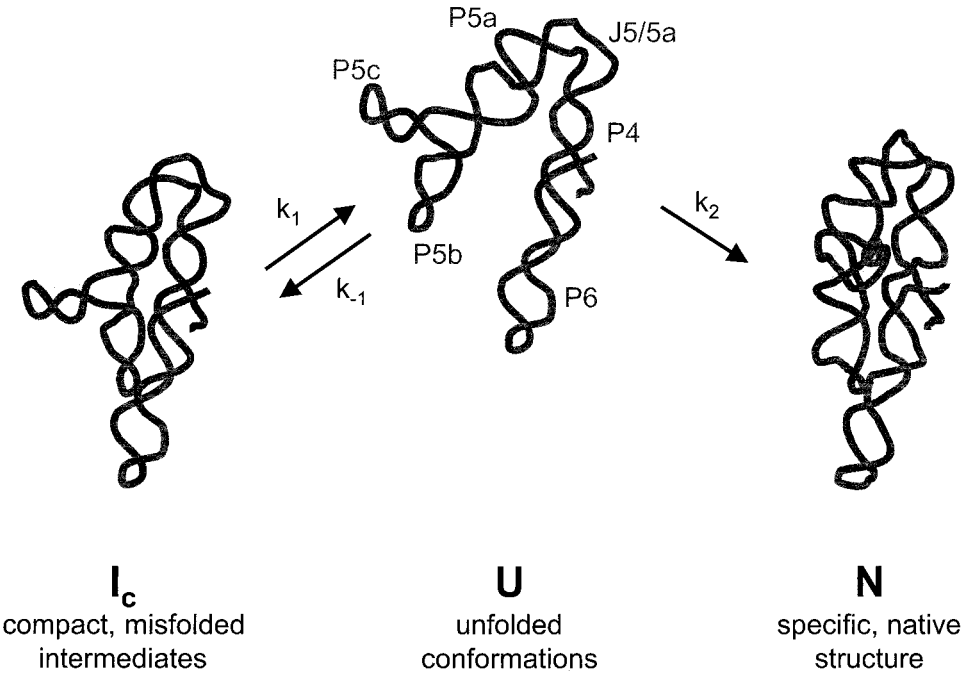

FIGURE 8: Folding mechanism of the P4−P6 domain. Unfolded P4−P6 RNA (U) is proposed to collapse to either the fully native tertiary structure (N) or to one or more compact conformations (I_c) in which P5abc is not properly folded. I_c may be less compact than N but is significantly more compact than U, thus impeding the folding of P5abc. At low ionic strength, I_c is favored over N, and the observed overall folding rate is 2 s^{-1}. At higher ionic strength, I_c is not detected, and N is formed at 15−31 s^{-1} (*19*).

folding and suggests that the same conformational transition underlies both phenomena. This conclusion is also supported by stopped-flow fluorescence studies of P4−P6 folding kinetics (*19*). Studies of $\bar{v}$ as a function of NaCl concentration for DNA (*33*) suggest that this value will not change more than several percent over the concentration range investigated here. Taken together, the centrifugation experiments suggest that increasing NaCl shifts the ensemble of unfolded RNA conformations to those that fold rapidly to the native structure.

DISCUSSION

Cooperativity of Tertiary Folding. The P4−P6 domain of the *Tetrahymena* ribozyme folds at lower Mg^{2+} concentrations (*27*) and at earlier times (*8*, *9*) than do sequences within the catalytic core of the ribozyme. To better understand early steps in the formation of RNA tertiary structure, the folding mechanism of the P4−P6 domain was probed by time-resolved hydroxyl radical footprinting using a synchrotron X-ray beam. The results showed that tertiary interactions in the isolated P4−P6 domain were formed twice as rapidly as in the whole ribozyme, consistent with equilibrium experiments showing that the domain folds autonomously (*10*). The domain may form more slowly in the context of the ribozyme because of interactions with nucleotides in other domains (*34*−*36*).

Folding of P4−P6 is highly cooperative, with tertiary interactions throughout the structure forming at similar rates and over a similar range of Mg^{2+} concentrations. Urea denaturation experiments also reveal a highly cooperative folding mechanism for P4−P6, with each of the tertiary contacts having similar stability (*37*). The equilibrium folding transition is fully saturated in 10 mM sodium cacodylate and 10 mM $MgCl_2$, the conditions used to measure the folding kinetics. The cooperativity of tertiary folding with respect to Mg^{2+} concentration is not unexpected, given the large number of ions that bind specific sites within the folded RNA. In electron density maps, as many as five divalent ions were localized within the P5abc subdomain and several additional ions were associated with the 150° bend in J5/5a and near the tetraloop (*38*). One of these binds to phosphate oxygens contributed by adjacent helices (*39*). Direct coordination of at least two Mg^{2+} to residues within the A-bulge is supported by the ability of Mn^{2+} ions to compensate for phosphorothioate substitutions in the RNA (*38*, *40*).

Rapid Formation of Tertiary Structure. In contrast to the wild-type P4−P6 RNA, the P5abc subdomain folds much more rapidly in the J5/5a paired and 72-nt P5abc RNAs that do not form long-range interactions between P5abc and the stacked P4/P6 helices. The extent of protection in P5c reached a plateau within the shortest initial time of our experiments (30 ms). From these data, it appears that the tertiary structure of the three-helix junction forms on time scales comparable to tertiary interactions in tRNA (10−100 ms) (*41*). As discussed below, the wild-type P4−P6 domain also folds in milliseconds when the ionic strength of the samples is increased. Time constants of less than 30 ms are consistent with the fast transitions monitored by changes in pyrene fluorescence (*19*) and most likely reflect the intrinsic rate at which the native tertiary structure is formed.

Non-Native Conformations Inhibit Folding. By contrast, the much slower folding of wild-type P4−P6 RNA in 10 mM sodium cacodylate implies that organization of the three-helix junction is inhibited under these conditions by interactions with other sequences in P4−P6. To account for this observation, a three-state mechanism is required (Figure 8). In this model, the initial population of unfolded RNA either collapses to the native structure (N) in the presence of Mg^{2+} or forms one or more compact conformations in which P5abc

is incorrectly folded (I_c). This could occur, for example, if P5c is mispaired in the initial population (*31*). The overall folding rate would be decreased if interactions in I_c inhibit refolding of P5c and must be partially disrupted for the native structure to form.

Competition between the native state (N) and a non-native, compact intermediate (I_c) could lower the observed folding rate in two ways. One possibility is that I_c is favored in the absence of Mg^{2+}. In this case, unfolding of I_c would be rate-limiting, and the rate constant for this step (I_c to U) should approach the observed rate of 2 s^{-1}. Alternatively, the extended U state is favored in the absence of Mg^{2+}, but I_c is formed much faster than N once the RNA is exposed to $MgCl_2$. If we assume that the intrinsic folding rate (U to N) is ~50 s^{-1}, I_c would have to be about 100-fold more stable than U to yield 2 s^{-1} overall.

The hydrodynamic properties obtained from the sedimentation studies suggest that the conformations of wild-type P4−P6 RNA and the mutant in which J5/5a is fully paired are very similar to each other in 10 mM sodium cacodylate. Therefore, it seems likely that the initial RNA population is in predominantly extended conformations under the low ionic strength conditions of our folding experiments. Instead, the sedimentation experiments support the second model, in which the average P4−P6 conformation is initially extended in the absence of Mg^{2+} (U) but then rapidly collapses to a non-native compact state (I_c) in the presence of Mg^{2+}. Since little native tertiary structure is detected at early times in the folding reaction, we presume that this initial collapse is nonspecific and that I_c contains a mixture of conformations.

The possibility that P4−P6 can adopt non-native, compact conformations upon the addition of Mg^{2+} is supported by the equilibrium hydroxyl radical protection pattern of U167C RNA (*32*). These experiments revealed that tertiary interactions between P5 and P5a still form even when P5abc is not correctly folded. Thus, the structure of the U167C mutant RNA may qualitatively resemble an intermediate conformation of the wild-type P4−P6 RNA. Although the junction between P5 and P5a is presumably flexible in the absence of Mg^{2+}, a comparison of J5/5a mutations concluded that the wild-type sequence predisposes the RNA toward the 150° bend observed in the native structure (*42*). Since disruption of the tetraloop−tetraloop receptor interaction had only a modest effect on the folding rate, this contact is presumably not critical to the stability of I_c.

Role of Monovalent Ions. Experiments that examine the effect of ionic strength on folding showed that the rate of forming N increases dramatically with increased sodium concentration. In 50−100 mM NaCl, P4−P6 is completely folded within 15 ms, as compared to ~500 ms in the absence of salt (*19*). Remarkably, the salt-dependent increase in the rate of folding corresponds precisely with the increases in the sedimentation and diffusion coefficients of P4−P6 RNA over the same range of NaCl concentrations (Figure 7b). Values of R_H decreased from 57 Å in the absence of added NaCl to 46 Å in 100 mM NaCl for the wild-type RNA (Table 3). From these results, we infer that the distribution of structures in the unfolded state is shifted toward conformations that are more compact when the ionic strength of the folding buffer is increased.

Since the sedimentation coefficients of the wild type and J5/5a paired RNAs were similar to each other in 0 and 100 mM additional NaCl, this conformational shift cannot be simply attributed to increased bending of J5/5a. Salt must enhance folding in other ways. One possibility is that P5c more easily adopts the native secondary structure, so that the probability of forming N in the presence of Mg^{2+} is increased. Another possibility is that competition between binding of Na^+ and Mg^{2+} ions to the RNA lowers the degree to which Mg^{2+} binding stabilizes non-native compact structures, thereby increasing the rate at which they rearrange to the native state. The degree of this competition is reflected in the increase in the midpoint of the Mg^{2+}-dependent folding transition from 0.3 to 2 mM with increasing NaCl (M.L.D., unpublished data). NaCl is known to increase the folding rate of the *Tetrahymena* pre-rRNA (*22*), while higher Mg^{2+} concentrations stabilize misfolded intermediates and lower the overall folding rate (*7*, *22*, *43*). Recently, small angle scattering experiments have demonstrated that binding of Mg^{2+} to RNA induces a rapid collapse to nonspecific, compact structures (*44*). At high monovalent ion concentrations, Na^+ ions may reduce the force of local electrostatic interactions, avoiding kinetically favored pathways that lead to incorrect intermediates. Instead, the population of RNA is distributed in conformations that can directly achieve the native state.

The results presented here demonstrate that the dominant kinetic folding mechanism of the stable P4-P6 domain is largely independent of other sequences in the *Tetrahymena* ribozyme. Although smaller structures, such as the P5abc subdomain of the ribozyme, form in milliseconds under all conditions tested so far, folding of the larger P4−P6 RNA is inhibited at low ionic strength. We propose that a tendency to form compact structures that are not native is the most plausible explanation for this inhibition, although other explanations, such as large-scale rearrangement of the secondary structure, cannot be completely dismissed. The considerable effect of Na^+ on the folding kinetics discussed here and in a companion paper (*19*) point to the vital role of both monovalent and divalent ions in the initial phases of the folding process.

ACKNOWLEDGMENT

We thank Elizabeth Doherty, Jennifer Doudna, Scott Silverman, Felicia Murphy, and Thomas Cech for the gift of plasmid and RNA; Yong Cao for T7 RNA polymerase; and Bianca Sclavi and Mike Sullivan for their assistance at beamline X9a. We also thank D. Thirumalai, Scott Silverman, and Thomas Cech for helpful discussion and communication of unpublished data; James C. Lee for assistance in the conduct and interpretation of the sedimentation velocity experiments; and John Philo for his support of SVEDBERG and for sharing much insight into analytical ultracentrifugation.

REFERENCES

1. Thirumalai, D., and Woodson, S. A. (1996) *Acc. Chem. Res. 29*, 433−439.
2. Pan, J., Thirumalai, D., and Woodson, S. A. (1997) *J. Mol. Biol. 273*, 7−13.
3. Pan, T., and Sosnick, T. R. (1997) *Nat. Struct. Biol. 4*, 931−938.
4. Treiber, D. K., Rook, M. S., Zarrinkar, P. P., and Williamson, J. R. (1998) *Science 279*, 1943−1946.

5. Pan, J., and Woodson, S. A. (1998) *J. Mol. Biol. 280*, 597−609.
6. Treiber, D. K., and Williamson, J. R. (1999) *Curr. Opin. Struct. Biol. 9*, 339−345.
7. Fang, X. W., Pan, T., and Sosnick, T. R. (1999) *Nat. Struct. Biol. 6*, 1091−1095.
8. Sclavi, B., Sullivan, M., Chance, M. R., Brenowitz, M., and Woodson, S. A. (1998) *Science 279*, 1940−1943.
9. Zarrinkar, P. P., and Williamson, J. R. (1994) *Science 265*, 918−924.
10. Murphy, F. L., and Cech, T. R. (1993) *Biochemistry 32*, 5291−5300.
11. Murphy, F. L., and Cech, T. R. (1994) *J. Mol. Biol. 236*, 49−63.
12. Cate, J. H., Gooding, A. R., Podell, E., Zhou, K., Golden, B. L., Kundrot, C. E., Cech, T. R., and Doudna, J. A. (1996) *Science 273*, 1678−1685.
13. Doherty, E. A., Herschlag, D., and Doudna, J. A. (1999) *Biochemistry 38*, 2982−2990.
14. Tullius, T. D., and Dombroski, B. A. (1986) *Proc. Natl. Acad. Sci. U.S.A. 83*, 5469−5473.
15. Tullius, T. D., and Dombroski, B. A. (1985) *Science 230*, 679−681.
16. Latham, J. A., and Cech, T. R. (1989) *Science 245*, 276−245.
17. Sclavi, B., Woodson, S., Sullivan, M., Chance, M., and Brenowitz, M. (1998) *Methods Enzymol. 295*, 379−402.
18. Silverman, S. K., and Cech, T. R. (1999) *Biochemistry 38*, 14224−14237.
19. Silverman, S. K., Deras, M. L., Woodson, S. A., Scaringe, S. A., and Cech, T. R. (2000) *Biochemistry*, submitted for publication.
20. Zaug, A. J., Grosshans, C. A., and Cech, T. R. (1988) *Biochemistry 27*, 8924−8931.
21. Ralston, C. Y., Sclavi, B., Sullivan, M., Deras, M. L., Woodson, S. A., Chance, M. R., and Brenowitz, M. (2000) *Methods Enzymol. 317*, 353−368.
22. Pan, J., Thirumalai, D., and Woodson, S. A. (1999) *Proc. Natl. Acad. Sci. U.S.A. 96*, 6149−6154.
23. Philo, J. S. (1997) *Biophys. J. 72*, 435−444.
24. Hinz, H.-J. (1986) *Thermodynamic Data for Biochemistry and Biotechnology*, Springer-Verlag, New York.
25. Sclavi, B., Woodson, S., Sullivan, M., Chance, M. R., and Brenowitz, M. (1997) *J. Mol. Biol. 266*, 144−159.
26. Banerjee, A. R., Jaeger, J. A., and Turner, D. H. (1993) *Biochemistry 32*, 153−163.
27. Celander, D. W., and Cech, T. R. (1991) *Science 251*, 401−407.
28. Russell, R., and Herschlag, D. (1999) *J. Mol. Biol. 291*, 1155−1167.
29. Joyce, G. F., van der Horst, G., and Inoue, T. (1989) *Nucleic Acids Res. 17*, 7879−7889.
30. van der Horst, G., Christian, A., and Inoue, T. (1991) *Proc. Natl. Acad. Sci. U.S.A. 88*, 184−188.
31. Wu, M., and Tinoco, I. (1998) *Proc. Natl. Acad. Sci. U.S.A. 95*, 11555−11560.
32. Silverman, S. K., Zheng, M., Wu, M., Tinoco, I., Jr., and Cech, T. R. (1999) *RNA 5*, 1665−1674.
33. Cohen, G., and Eisenberg, H. (1968) *Biopolymers 6*, 1077−1100.
34. Pan, J., and Woodson, S. A. (1999) *J. Mol. Biol. 294*, 955−965.
35. Doherty, E. A., and Doudna, J. A. (1997) *Biochemistry 36*, 3159−3169.
36. Golden, B. L., Gooding, A. R., Podell, E. R., and Cech, T. R. (1988) *Science 282*, 259−264.
37. Ralston, C. Y., He, Q., Brenowitz, M., and Chance, M. R. (2000) *Nat. Struct. Biol. 7*, 371−374.
38. Cate, J. H., Hanna, R. L., and Doudna, J. A. (1997) *Nat. Struct. Biol. 4*, 553−558.
39. Cate, J. H., Gooding, A. R., Podell, E., Zhou, K., Golden, B. L., Szewczak, A. A., Kundrot, C. E., Cech, T. R., and Doudna, J. A. (1996) *Science 273*, 1696−1698.
40. Basu, S., and Strobel, S. A. (1999) *RNA 5*, 1399−1407.
41. Draper, D. E. (1996) *Nat. Struct. Biol. 3*, 397−400.
42. Szewczak, A. A., and Cech, T. R. (1997) *RNA 3*, 838−849.
43. Rook, M. S., Treiber, D. K., and Williamson, J. R. (1999) *Proc. Natl. Acad. Sci. U.S.A. 96*, 12471−12476.
44. Russell, R., Millett, I. S., Doniach, S., and Herschlag, D. (2000) *Nat. Struct. Biol. 7*, 367−370.
45. Cech, T. R., Damberger, S. H., and Gutell, R. R. (1994) *Nat. Struct. Biol. 1*, 273−280.

BI0010118